

# A Dynamic, Adaptive, Locally Conservative and Nonconforming Solution Strategy for Transport Phenomena in Chemical Engineering

Shuyu Sun and Mary F. Wheeler

*The Institute for Computational Engineering and Sciences (ICES)  
The University of Texas, Austin, Texas 78712, USA*

**Abstract:** A family of discontinuous Galerkin (DG) methods are formulated and applied to chemical engineering problems. They are the four primal discontinuous Galerkin schemes for the space discretization: Symmetric Interior Penalty Galerkin, Oden-Baumann-Babuska DG formulation, Nonsymmetric Interior Penalty Galerkin and Incomplete Interior Penalty Galerkin. Numerical examples of DG to solve typical chemical engineering problems, including a diffusion-convection-reaction system in a catalytic particle, a problem of heat transfer in a fixed bed and a contaminant transport problem in porous media, are presented. This paper highlights the substantial advantages of DG on adaptive mesh modification over traditional methods. In particular, we formulate and study the dynamic mesh modification strategy for DG guided by mathematically sound *a posteriori* error estimators.

**Keywords:** Discontinuous Galerkin Methods, Transport Phenomena, Parabolic Partial Differential Equations, Dynamic Mesh Adaptation.

## 1. Introduction

Transport phenomena, including mass, momentum and heat transfer and the coupling of transport and chemical reactions, play a dominant role in chemical engineering processes. For example, a distillation process in a packed column involves fluid flow (momentum transfer) of liquid and vapor phases, mass transfer within a homogeneous phase and on the liquid and vapor interface, and heat transfer within and between phases [6, 9-11, 16]. Mathematical modeling of transport phenomena has been widely employed in many areas of chemical engineering. Analytical solutions for such modeling systems are usually not available due to the complexity of the chemical engineering process systems. Instead, numerical methods have to be used extensively.

Finite difference methods (FDMs), in particular the cell center finite difference methods, are widely used for numerical simulation of transport phenomena arising in chemical engineering due to the simplicity of implementation. However, FDMs have many limitations. They are difficult to handle complex geometry of the domain. FDMs are generally lower order methods and cannot directly handle full tensor parameters (e.g. anisotropic diffusivity, conductivity or permeability). Moreover, FDMs do not provide the flexibility of locally mesh adaptation without using complicated arguments. Finite volume methods (FVMs) and finite element methods (FEMs) are two families of solution strategies that are flexible for the treatment of complex geometry and local mesh refinement, and are widely used in the field of computational fluid dynamics (CFD). The traditional FEMs (the continuous Galerkin methods), however, are not locally conservative without post-processing. FVMs, by design, preserve locally conservation, but they are generally low-order methods and are complicated to extend to high-order approximations. In addition, FVMs are difficult to treat full tensor parameters.

Discontinuous Galerkin (DG) methods are specialized finite element methods that utilize discontinuous spaces to approximate solutions [2, 4-5, 7-8, 12-15, 17-18]. DG methods have recently gained popularity for many attractive properties. First of all, the methods are locally conservative while most classical finite element methods are not. In addition, they have less numerical diffusion than most conventional algorithms, thus are likely to offer more accurate solutions, especially for convection-dominated transport problems. They handle rough coefficient problems and capture the discontinuity in the solution very well by the nature of discontinuous function spaces. DG can naturally handle inhomogeneous boundary conditions and curved boundaries. Furthermore, with appropriate meshing, DG is capable of delivering exponential rates of convergence. For time-dependent problems in particular, the mass matrices are block diagonal for DG, but not for conforming methods. This provides DG a substantial computational advantage, especially if explicit time integrations are used. However, the applications of DG to chemical engineering problems are still limited.

In this paper, we consider a family of DG methods applied to chemical engineering problems. They are the four primal discontinuous Galerkin schemes for the space discretization: Symmetric Interior Penalty Galerkin (SIPG) [7, 17], Oden-Baumann-Babuska version of DG (OBB-DG) [4], Nonsymmetric Interior Penalty Galerkin (NIPG) [5] and Incomplete Interior Penalty Galerkin (IIPG) methods [2, 7]. Formulation of these schemes will be first introduced to a general time-dependent parabolic type equation, and then applied to the simulation of transport and reaction arising from chemical engineering. Three representative chemical engineering problems, namely, a diffusion-convection-reaction problem in a catalytic particle, a problem of heat transfer in a fixed bed and a contaminant transport problem in porous media, will be presented. Efficient implementation issues and advantages of DG will be addressed. In particular, the dynamic mesh adaptation strategies are proposed, by which the local physical phenomena can be effectively and efficiently captured.

## 2. Model Equation and Discontinuous Galerkin Algorithms

We let  $\Omega$  be a polygonal and bounded domain in a  $d$ -dimensional space ( $d=1, 2$  or  $3$ ), and let  $T$  be the final simulation time. We consider the following general parabolic equation:

$$\frac{\partial \phi c}{\partial t} + \nabla \cdot (\mathbf{u}c - \mathbf{D}\nabla c) = r(c), \quad (x, t) \in \Omega \times (0, T], \quad (1)$$

where the dependent (unknown) variable is  $c$ . Here,  $\phi$ , a scalar,  $\mathbf{u}$ , a vector, and  $\mathbf{D}$ , a second-order tensor, are given data, and can be functions of time and space. The right hand side  $r(c)$  is a given function of the unknown variable  $c$ , and can be functions of time and space as well:  $r(c)=r(c, x, t)$ . Equation (1) can be used to model transport phenomena including heat and mass transfer processes. For example, to model single-phase contaminant transport in porous media, the unknown variable  $c$  is considered as the concentration of a species (amount per volume);  $\phi$  is the porosity;  $\mathbf{u}$  is the Darcy velocity;  $\mathbf{D}$  is the dispersion/diffusion tensor;  $r(c)$  is the term from well injection, extraction and chemical reaction. More variations of the model equation will be presented in the numerical example sections of this paper.

We consider two types of general boundary conditions: the Dirichlet and the Robin types. We divide the domain boundary  $\partial\Omega$  into the Dirichlet boundary  $\Gamma_D$  and the Robin

boundary  $\Gamma_R$  such that  $\Gamma_D \cap \Gamma_R = \emptyset$  and  $\bar{\Gamma}_D \cup \bar{\Gamma}_R = \partial\Omega$ . The following boundary conditions are imposed for the problem (1):

$$c(x, t) = c_B, \quad x \in \Gamma_D, t \in (0, T], \quad (2)$$

$$-\mathbf{D}\nabla c \cdot \mathbf{n} = k_B(c - c_B), \quad x \in \Gamma_R, t \in (0, T], \quad (3)$$

where  $c_B$  and  $k_B$  are given boundary data that can be constants or functions of time and boundary space. We impose the following initial condition:

$$c(x, 0) = c_0, \quad (4)$$

where  $c_0$  is the given initial data that could be a function of space. We remark that the inflow, outflow and no-flow boundary conditions employed in modeling contaminant transport problems (see [7-8, 12-15] as well as Section 5 of this paper) are special cases of the Robin boundary condition (3).

To discretize the space, we let  $E_h$  be a family of non-degenerate and possibly non-conforming partitions of the domain  $\Omega$  composed of line segments for one-dimensional space, triangles and/or quadrilaterals for two-dimensional space, or tetrahedral, prisms and/or hexahedra for three-dimensional space. The set of interior element interfaces is denoted by  $\Gamma_h$ . We define the average and the jump for an element-wise smooth function on the interface  $\gamma$  of two elements  $e_1$  and  $e_2$  as follows.

$$\{\phi\} = \frac{1}{2} \left( \left( \phi|_{e_1} \right)_{|\gamma} + \left( \phi|_{e_2} \right)_{|\gamma} \right),$$

$$[\phi] = \left( \phi|_{e_1} \right)_{|\gamma} - \left( \phi|_{e_2} \right)_{|\gamma}.$$

The discontinuous finite element space is taken to be

$$D_r(E_h) = \{f \in L^2(\Omega) : f|_e \in P_r(e), \forall e \in E_h\},$$

where  $P_r(e)$  denotes the space of polynomials of (total) degree less than or equal to  $r$  on the element  $e$ .

We introduce the bilinear form  $B(c, w)$  as follows:

$$\begin{aligned} B(c, w) = & \sum_{e \in E_h} \int_e (\mathbf{D}\nabla c - \mathbf{c}\mathbf{u}) \cdot \nabla w - \sum_{\gamma \in \Gamma_h} \int_{\gamma} \{\mathbf{D}\nabla c \cdot \mathbf{n}\} [w] - s_{form} \sum_{\gamma \in \Gamma_h} \int_{\gamma} \{\mathbf{D}\nabla w \cdot \mathbf{n}\} [c] \\ & + \sum_{\gamma \in \Gamma_h} \int_{\gamma} c^* \mathbf{u} \cdot \mathbf{n} [w] - \sum_{\gamma \subset \Gamma_D} \int_{\gamma} \mathbf{D}\nabla c \cdot \mathbf{n} w - s_{form} \sum_{\gamma \subset \Gamma_D} \int_{\gamma} \mathbf{D}\nabla w \cdot \mathbf{n} c \\ & + \sum_{\gamma \in \Gamma_D \cup \Gamma_R} \int_{\gamma} \mathbf{c}\mathbf{u} \cdot \mathbf{n} w + \sum_{\gamma \subset \Gamma_R} \int_{\gamma} k_B c w + \sum_{\gamma \in \Gamma_h} \frac{r^2 \sigma_{\gamma}}{h_{\gamma}} \int_{\gamma} [c] [w], \end{aligned} \quad (5)$$

where  $c^*$  is the upwind value of  $c$ , and  $s_{form}$  is taken to be -1 for NIPG and OBB-DG, 1 for SIPG, and 0 for IIPG. Penalty parameters ( $\sigma_{\gamma}$ ) are zero for OBB-DG, nonnegative for NIPG, and strictly positive for SIPG and IIPG. The linear functional  $L(w; c)$  is defined as

$$L(w; c) = \int_{\Omega} r(c) w - s_{form} \sum_{\gamma \subset \Gamma_D} \int_{\gamma} \mathbf{D}\nabla w \cdot \mathbf{n} c_B + \sum_{\gamma \subset \Gamma_R} \int_{\gamma} k_B c_B w. \quad (6)$$

The continuous-in-time DG solution  $C^{DG} \in W^{1, \infty}(0, T; D_r(E_h))$  of the problem (1)-(4) is given by

$$\left( \frac{\partial \phi C^{DG}}{\partial t}, w \right) + B(C^{DG}, w) = L(w; C^{DG}), \quad \forall w \in D_r(E_h), \forall t \in (0, t], \quad (7)$$

$$(\phi C^{DG}, w) = (\phi c_0, w), \quad \forall w \in D_r(E_h), t = 0. \quad (8)$$

A fully discretized DG algorithm can be obtained from the above formulation by further applied a standard time integration scheme such as the backward Euler method, the trapezoid rule or a Runge-Kutta method.

Four different primal DG schemes, i.e. OBB-DG, NIPG, SIPG and IIPG, are unified in a single formulation (7)-(8), depending upon the choice of  $s_{form}$  and the penalty term. The algorithm (7)-(8) is known to possess local conservative property (element-wise satisfaction of mass/heat/momentum balance) [2, 5, 7, 15]. The existence of a unique solution of the equation system (7)-(8) has been mathematically established [7]. It is shown [5] that the error in the  $L^2(H^1)$  norm from OBB-DG converges optimally in  $h$  (the mesh size) and nearly optimally in  $p$  (the degree of approximation):

$$\left\| \sqrt{\phi} (C^{DG} - c) \right\|_{L^\infty(L^2)} + \left\| \mathbf{D}^{1/2} \nabla (C^{DG} - c) \right\|_{L^2(L^2)} \leq K \frac{h^{\min(r, s-1)}}{r^{\frac{s-5}{2}}},$$

where  $C^{DG}$  is the DG solution,  $c$  the exact solution,  $r$  the order of approximation,  $h$  the maximum element length, and  $s$  the regularity of the solution. The positive constant  $K$  depends upon only the solution, and is independent of the mesh size and the order of approximation. Because of the penalty term, the convergence of NIPG, IIPG and SIPG in the  $L^2(H^1)$  norm is not only optimally in  $h$ , but also is closer to optimality in  $p$  [7]:

$$\left\| \sqrt{\phi} (C^{DG} - c) \right\|_{L^\infty(L^2)} + \left\| \mathbf{D}^{1/2} \nabla (C^{DG} - c) \right\|_{L^2(L^2)} \leq K \frac{h^{\min(r, s-1)}}{r^{\frac{s-3}{2}}}.$$

If the mesh is conforming and contains only line segments, triangles or tetrahedral, NIPG, IIPG and SIPG achieve optimal  $L^2(H^1)$  convergence in both of  $h$  and  $p$  [7]. It should be pointed out that SIPG is the only primal DG method that possesses optimal  $L^2(L^2)$  convergence in  $h$  [7]:

$$\left\| \sqrt{\phi} (C^{DG} - c) \right\|_{L^2(L^2)} \leq K \frac{h^{\min(r+1, s)}}{r^{\frac{s-3}{2}}}.$$

Because of this optimality in  $L^2(L^2)$  norm, the SIPG method is a particularly interesting DG method, especially if the scalar unknown variable  $c$  is of primary interest rather than its flux. SIPG is also interesting from a computational point of view since, it is the only DG method that gives a symmetric algebraic system for diffusion-reaction type equations, which could be exploited to construct fast linear solvers. Other family members of primal DG methods are of interest as well in many situations. For instance, OBB-DG and NIPG methods are capable to handle problems involving high varying coefficients, and IIPG is the only fully compatible method among the four for coupled flow and transport problems [2, 7, 15].

### 3. Two Numerical Examples without Mesh Adaptation

#### 3.1. A Diffusion-Convection-Reaction System in a Catalytic Particle

We first apply DG to the classic chemical engineering problem concerning diffusion-convection and reaction in a catalytic particle [1]. The model equation is given by

$$\frac{\partial c}{\partial t} = \frac{\partial^2 c}{\partial x^2} - \lambda_m \frac{\partial c}{\partial x} - \Phi^2 c, \quad 0 < x < 2, t > 0.$$

The variable  $c$ , a normalized concentration, is a function of time  $t$  and one-dimensional space  $x$ . We note that, even though physical phenomena occur in a three-dimensional space, the model equation reduces to a one spatial dimension by taking advantage of the symmetry of the problem. The variable  $t$  is the time normalized by the diffusion time constant. Similarly, the space variable  $x$  has been normalized by the half thickness of the particle.  $\lambda_m$  is the intraparticle Peclet number and  $\Phi$  is the Thiele module. We impose the normalized boundary and initial conditions:

$$\begin{aligned} c(x, 0) &= 0, & 0 < x < 1, \\ c(0, t) &= c(2, t) = 1, & t > 0. \end{aligned}$$

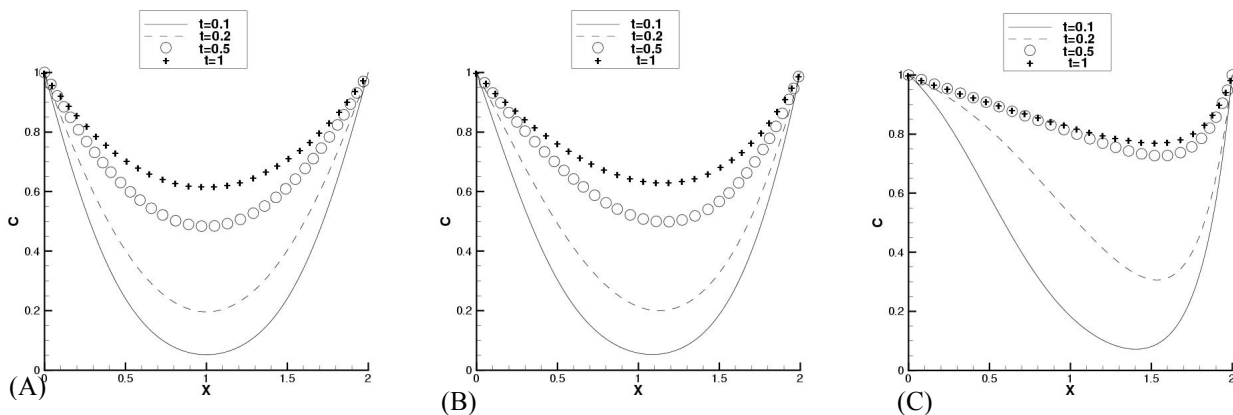


**Figure 1.** Effect of the intraparticle Peclet number on concentration profiles ( $\Phi = 1$ ):  
(A)  $\lambda_m = 0$ , (B)  $\lambda_m = 1$ , (C)  $\lambda_m = 5$ .

Simulations are conducted for different values of parameters  $\lambda_m$  and  $\Phi$  in order to test the performance of the algorithm. To demonstrate that DG works well even without mesh adaptation, we use a uniform grid with 100 elements. Though the other three DG schemes could be used as well, OBB-DG is chosen for this numerical example. OBB-DG is more convenient than the other three in the sense that it does not contain the penalty term, thus eliminate the choice of penalty parameters. The complete quadratic basis functions (i.e.  $r=2$ ) are used for each element. The backward Euler method with a uniform time step  $\Delta t = 0.01$  is used for time integration. Concentration profiles are plotted in Figures 1 and 2 at various times,

from  $t=0.1$  to  $t=1$ , with various combination of model parameters. Figure 1 compares the concentration profiles for different intraparticle Peclet numbers. We remark that Figure 1(A) displays the behavior of the diffusion-reaction system in absence of convection. Figure 2 illustrates the influence of the Thiele modules on concentration profiles. Clearly, the behaviors of the diffusion-convection-reaction system are thoroughly reproduced by the DG scheme in a wide range of system parameters. In addition, it is shown that DG is effective to both the convection-free diffusion-reaction system (Figure 1(A)) and the convection-dominated diffusion-convection-reaction problem (Figure 2(A)), as well as the reaction-dominated system (Figure 2(F)).

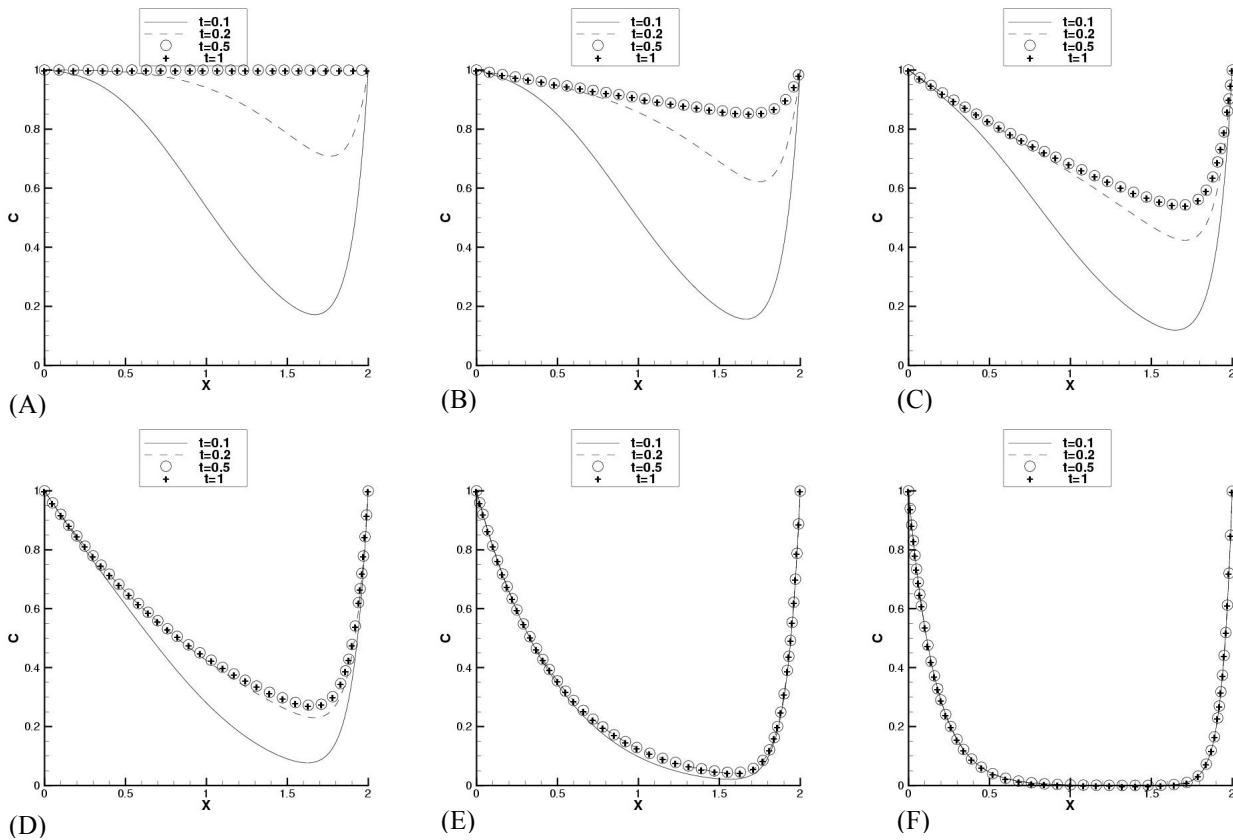


**Figure 2.** Effect of the Thiele module on concentration profiles ( $\lambda_m = 10$ ):  
 (A)  $\Phi = 0$ , (B)  $\Phi = 1$ , (C)  $\Phi = 2$ , (D)  $\Phi = 3$ , (E)  $\Phi = 5$ , (F)  $\Phi = 10$ .

### 3.2. A Heat Transfer Process in a Fixed Bed

The study of heat transfer in fixed beds is of considerable importance in various unit operations in chemical engineering. In particular, simulation of this process is crucial to the analysis and design of separation units in which a fluid passing through the bed exchanges mass and heat with the particles in the presence of chemical reactions (e.g. exothermic catalytic reaction) or in the absence of chemical reactions (e.g. non-isothermal adsorption).

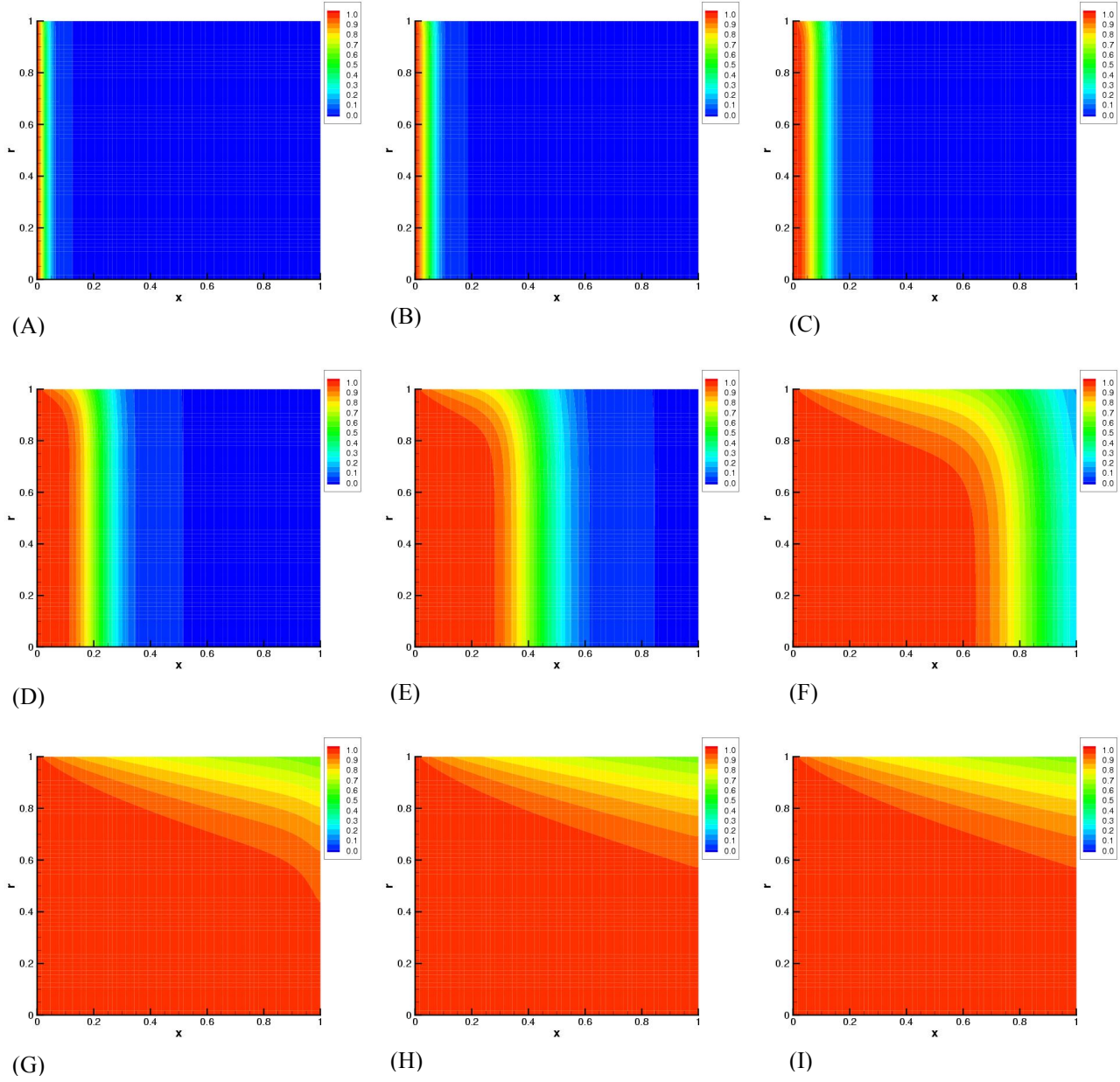


**Figure 3.** Normalized temperature profiles at various times: (A)  $t = 0.05$ , (B)  $t = 0.1$ , (C)  $t = 0.2$ , (D)  $t = 0.5$ , (E)  $t = 1$ , (F)  $t = 2$ , (G)  $t = 3$ , (H)  $t = 4$ , (I)  $t = 10$ .

We now consider a two-dimensional pseudo-homogeneous model described by the following governing dimensionless equation [1, 3]:

$$(1 + \xi_h) \frac{\partial T}{\partial t} = \frac{1}{Pe_h} \frac{\partial^2 T}{\partial x^2} + \frac{L}{Pe_r} \frac{\partial^2 T}{\partial r^2} - \frac{\partial T}{\partial x} + \frac{L}{r Pe_r} \frac{\partial^2 T}{\partial r^2},$$

$$0 < x < 1, 0 < r < 1, t > 0,$$

where  $T$  is the dimensionless temperature,  $x$  the normalized axial variable along the fixed bed,  $r$  the normalized radial variable and  $t$  the dimensionless time. There are four dimensionless

parameters in the differential equation:  $\xi_h$ , the thermal capacity factor,  $Pe_h$ , the axial thermal Peclet number,  $Pe_r$ , the radial thermal Peclet number, and  $L$ , the ratio of the bed length and radius. There is one more dimensionless number,  $Bi$ , the thermal Biot number, in the following imposed boundary conditions:

$$\begin{aligned} T(0,r,t) &= 1, & 0 \leq r < 1, t > 0, \\ \frac{\partial T}{\partial x}(1,r,t) &= 0, & 0 \leq r < 1, t > 0, \\ \frac{\partial T}{\partial r}(x,0,t) &= 0, & 0 < x < 1, t > 0, \\ \frac{\partial T}{\partial r}(x,1,t) &= -BiT(x,1,t), & 0 < x < 1, t > 0. \end{aligned}$$

The initial condition is given by

$$T(x,r,0) = T_0, \quad 0 < x < 1, 0 \leq r < 1.$$

We carry out the simulation with the following parameters:  $\xi_h = 1.3$ ,  $Pe_h = 100$ ,  $Pe_r = 500$ ,  $L = 20$ ,  $Bi = 8$  and  $T_0 = 0$ . We use OBB-DG for this numerical example and remark that the other three DG schemes could be applied as well. A uniform 32 by 32 mesh with the complete quadratic basis functions for each element is used for spatial discretization. The backward Euler method with a uniform time step  $\Delta t = 0.01$  is used for time integration. Temperature profiles are presented in Figures 3 at various times, from  $t=0.05$  to  $t=10$ . It is easy to see that the enthalpy (heat energy) is transferred into the bed mainly by convection at the entrance of the bed, and is transferred out of the bed by both the conduction through the wall and the convection at the bed exit. Inside the bed, heat transfer is dominated by convection in early times and is balanced by convection and conduction at later times. The temperature profile ultimately approaches a steady state, where heat is transferred in radial direction only by conduction and in axial direction mainly by convection. This numerical example demonstrates that DG is effective for both the conduction dominated and the convection dominated problems.

#### 4. Mesh Adaptation Strategies

Mesh modification is an important ingredient of adaptive strategies for FEMs. DG possesses substantial advantages over classic FEMs in term of adaptive mesh modification. First of all, the approximation spaces for DG are localized in each element, which provides a flexibility allowing for general non-conforming meshes with variable degree of approximation. In particular, non-matching grids and hanging nodes are treated naturally in DG. This results in substantially easier adaptive implementation for DG than for conventional FEM approaches. This flexibility also increases the efficiency of adaptivity because the unnecessary areas do not need to be refined in order to maintain conformity of the mesh.

For any adaptive mesh modification, we need to know which set of elements need to be refined or coarsened to improve our solution. This goal is often achieved by an *a posteriori* error estimate (or error indicator), which provides valuable error information, and can be used

to guide adaptive modifications of the mesh. Using a duality argument, we have developed an explicit  $L^2(L^2)$  *a posteriori* error estimate for SIPG applied to time-dependent problems (see [7, 12] for detailed information):

$$\|\sqrt{\phi}(C^{DG} - c)\|_{L^2(L^2)} \leq K \left( \sum_{e \in E_h} \eta_e^2 \right)^{1/2},$$

where the local error indicator  $\eta_e$  is defined by

$$\begin{aligned} \eta_e^2 &= \frac{h_e^4}{r^4} \|R_I\|_{L^2(L^2(e))}^2 + \frac{1}{2} \sum_{\gamma \in \partial e \setminus \partial \Omega} \left( \frac{h_\gamma}{r} + \delta r h_\gamma \right) \|R_{B0}\|_{L^2(L^2(\gamma))}^2 \\ &\quad + \frac{1}{2} \sum_{\gamma \in \partial e \setminus \partial \Omega} \left( \frac{h_\gamma^3}{r^3} \|R_{B1}\|_{L^2(L^2(\gamma))}^2 \right) + \sum_{\gamma \in \partial e \cap \partial \Omega} \left( \frac{h_\gamma^3}{r^3} \|R_{B1}\|_{L^2(L^2(\gamma))}^2 \right). \end{aligned}$$

This *a posteriori* error estimate is especially valuable in the cases where the primal scalar unknown rather than the flux is of interest. It is easy to implement and computationally cheap. Numerical experiments show that it is sharp in capturing the areas with large errors and could guide effective mesh modifications to achieve efficient adaptivities [12]. In particular, they are sharp in capturing concentration fronts in reactive transport problems. As for the other primal DG schemes, we have established a unified *a posteriori* error estimate approach in the  $L^2(H^1)$  norm (see [7, 14] for detailed information):

$$\|\sqrt{\phi}(C^{DG} - c)\|_{L^\infty(L^2)} + \|\mathbf{D}^{1/2}(\mathbf{u}) \nabla(C^{DG} - c)\|_{L^2(L^2)} \leq K \left( \sum_{e \in E_h} \eta_e^2 \right)^{1/2},$$

where the local error indicator  $\eta_e$  is defined by

$$\begin{aligned} \eta_e^2 &= h_e^2 \|R_I\|_{L^2(L^2(e))}^2 + \sum_{\gamma \in \partial e \cap \partial \Omega} h_\gamma \|R_{B1}\|_{L^2(L^2(\gamma))}^2 \\ &\quad + \frac{1}{2} \sum_{\gamma \in \partial e \setminus \partial \Omega} h_\gamma \|R_{B1}\|_{L^2(L^2(\gamma))}^2 + \frac{1}{2} \sum_{\gamma \in \partial e \setminus \partial \Omega} \frac{1}{h_\gamma} \|R_{B0}\|_{L^2(L^2(\gamma))}^2 \\ &\quad + \frac{1}{2} \sum_{\gamma \in \partial e \setminus \partial \Omega} h_\gamma \|R_{B0}\|_{L^\infty(L^2(\gamma))}^2 + \frac{1}{2} \sum_{\gamma \in \partial e \setminus \partial \Omega} h_\gamma \|\partial R_{B0} / \partial t\|_{L^2(L^2(\gamma))}^2. \end{aligned}$$

The approach is flexible and applies to all the four versions of DG, namely, OBB-DG, SIPG, NIPG and IIPG. The *a posteriori* error estimates in  $L^2(H^1)$  is explicit and residual based, and thus is also computationally efficient. General boundary conditions can be easily incorporated into these  $L^2(H^1)$  error estimates. In addition, no regularity assumption for the dual problem is required for these estimates. Numerical performance of the *a posteriori* error estimators under two major categories, namely estimators in  $L^2(L^2)$  and in  $L^2(H^1)$  have been investigated and compared [7, 12, 14]. Results indicate that  $L^2(H^1)$  type error indicator is more flexible, but  $L^2(L^2)$  type error indicator is more effective for many reactive transport cases.

We consider two types of mesh modifications: mesh enrichment and mesh adjustment. In the first approach, a set of elements in the mesh are chosen to be refined according to an error indicator. Figure 4 illustrates the approach, where the three elements with the largest error indicator values are locally refined. The number of elements in the mesh grows after an application of mesh enrichment. Alternatively, in mesh adjustment, we can fix the number of elements, but refine some elements and coarsen some other elements adaptively to make the mesh more suitable for the problem. Figure 5 gives an example of this approach, where the

three elements with the largest error indicator values are locally refined while the other three elements with the smallest error indicator values are locally coarsened, and the total number of elements remains constant.

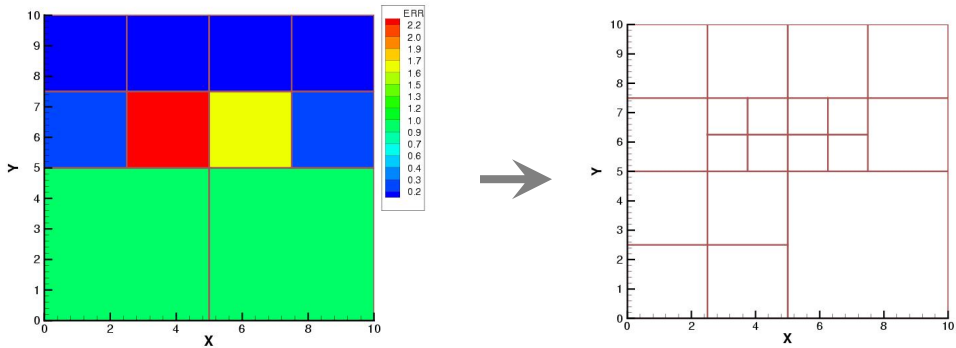


**Figure 4.** Illustration of the mesh enrichment approach.

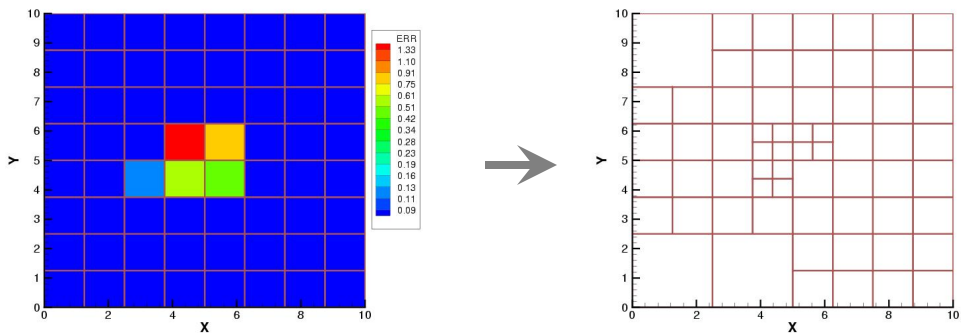


**Figure 5.** Illustration of the mesh adjustment approach.

There are mainly two types of mesh adaptation strategies: static and dynamic ones. In a static adaptive approach, we usually start with a coarse mesh and increase the number of elements by mesh enrichment according to an error indicator [7, 13]. On the other hand, a dynamic adaptive strategy is often to start with a fine mesh and modify the mesh with time steps using mesh adjustment according to an error indicator [13]. A static strategy is mainly used for time-independent problems, and it generates a single adaptive mesh for all time, if applied to transient problems. A dynamic strategy is associated with time-dependent problems and produces adaptive meshes dynamically changed with time.

Dynamic mesh modifications are particularly effective for transient problems involving a long period of simulation time, because the location of strong physics usually moves with time. It is favorable to compute the error indicator for only a short time interval involving the current time, and to modify the mesh dynamically with time. Because it is expensive to change the mesh each time step, we divide the entire simulation time into a collection of time slices, each of which may in turn contains a certain number of time steps. Our dynamic mesh adaptation strategy for DG is detailed in Algorithm 1. We note that a coarsening-compatible condition is enforced in Algorithm 1 to ensure the consistency of mesh data structure. Unlike in conforming FEM methods, each element in the DG mesh may be refined since DG allows

for an arbitrary degree of nonconformity. However, not every element is available to be coarsened; for instance, the element without a father cannot be further coarsened. The coarsening-compatible condition is defined in Definition 1.

**Algorithm 1.** (Dynamic mesh adaptation for DG)

Given an initial mesh  $E_0$ , a modification factor  $\alpha \in (0,1)$ , time slices  $\{(T_0, T_1), (T_1, T_2), \dots, (T_{N-1}, T_N)\}$  and iteration numbers for each time slices  $\{M_1, M_2, \dots, M_N\}$ .

1. Let  $n = 1$ ;
2. Let  $m = 1$ ;
3. Compute the initial solution for time slice  $(T_{n-1}, T_n)$  using either the initial condition (if  $n = 1$ ) or the solution at the end of last time slice (if  $n > 1$ ) by a local projection;
4. Let  $E_{m,n} = E_0$  if  $n=1$  and  $m=1$ ; or  $E_{m,n} = E_{M_{n-1}+1, n-1}$  if  $n > 1$  and  $m=1$ ;
5. Compute the DG approximation of the PDE for the time slice  $(T_{n-1}, T_n)$  based on the mesh  $E_{m,n}$  and compute the error indicator  $\eta_e$  for each element  $e \in E_{m,n}$ ;
6. Select  $E_r \subset E_{m,n}$  such that
 
$$\#(E_r) = \text{round}(\alpha \#(E_{m,n})) \text{ and } \min\{\eta_e : e \in E_r\} \geq \max\{\eta_e : e \in E_{m,n} \setminus E_r\};$$
7. Select  $E_c \subset E_{m,n}$  to minimize  $\max\{\eta_e : e \in E_c\}$  subject to
 
$$\#(E_c) = \text{round}(\alpha \#(E_{m,n}))$$
 and that  $E_c$  satisfies the coarsening-compatible condition with regard to  $E_{m,n}$  and  $E_r$ ;
8. Refine all elements  $e \in E_r$  and coarsen all elements  $e \in E_c$  to form a new mesh  $E_{m+1,n}$ ;
9. Let  $m=m+1$ . If  $m \leq M_n$ , go to step 3;
10. Let  $n=n+1$ . If  $n \leq N$ , go to step 2;
11. Report the solution and stop.

**Definition 1.** (Coarsening-compatible condition)

The coarsening element set  $E_c$  is said to satisfy the coarsening-compatible condition with regard to the mesh  $E$  and the refining element set  $E_r$  if and only if the following conditions are satisfied:

1. Each element in  $E_c$  has a father;
2. Brothers of an element in  $E_c$  are active, that is, they sit in  $E$ ;
3. None of the elements in  $E_c$  and their brothers are in  $E_r$ ;
4. Brothers of an element in  $E_c$  are not in  $E_c$ .

## 5. A Numerical Example with Dynamic Mesh Adaptation

We consider the following normalized contaminant transport problem in a single phase in porous media:

$$\begin{aligned} \frac{\partial \phi_e c}{\partial t} + \nabla \cdot (\mathbf{u}c - \mathbf{D}\nabla c) &= 0, & (x, t) \in \Omega \times (0, T], \\ (\mathbf{u}c - \mathbf{D}\nabla c) \cdot \mathbf{n} &= c_B \mathbf{u} \cdot \mathbf{n}, & (x, t) \in \Gamma_{in} \times (0, T], \\ (-\mathbf{D}\nabla c) \cdot \mathbf{n} &= 0, & (x, t) \in \Gamma_{out} \times (0, T], \\ c(x, 0) &= c_0(x), & x \in \Omega, \end{aligned}$$

where the domain  $\Omega = (0, 10)^2$  has an inflow boundary  $\Gamma_{in}$  and an outflow/no-flow boundary  $\Gamma_{out}$ . The diffusion-dispersion  $\mathbf{D}$  is a constant, diagonal tensor with  $D_{ij} = 0.01$ ; and the velocity is  $\mathbf{u} = (-0.1, 0)$  uniformly across the domain. The domain  $\Omega$  is divided into two parts, i.e. the lower half  $\Omega_l = (0, 10) \times (0, 5)$  and the upper half  $\Omega_u = (0, 10) \times (5, 10)$ . The effective porosity  $\phi_e$  in  $\Omega_u$  is 0.1. Adsorption occurs only in the lower part of the domain, which results in an effective porosity  $\phi_e = 0.2$  in  $\Omega_l$ . The initial total concentration is 0.1 inside the square centered at (5,5) with the size of  $0.3125 \times 0.3125$  and is 0.0 elsewhere, as shown in Figure 6(A). The total concentration here is defined as the product of the concentration in fluid and the effective porosity.

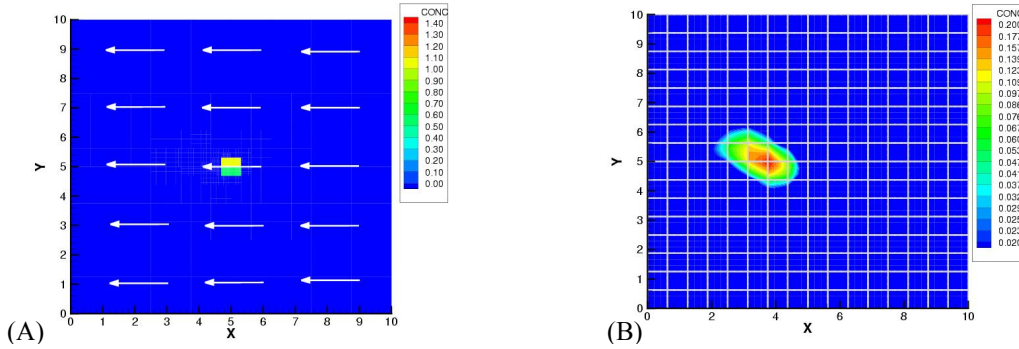


**Figure 6.** Numerical example of contaminant transport in porous media: (A) velocity and initial contaminant concentration in fluid, (B) DG solution at  $t=1$  using a uniform rectangular mesh without mesh adaptation

SIPG is employed to solve this problem because the scalar variable (concentration) is of primal interest in this problem and SIPG is only one of the four primal DG methods that possesses optimal *a priori* and *a posteriori* error estimators in  $L^2(L^2)$ . The penalty parameter is chosen according to [7]. The simulation time interval is  $(0, 2)$  and we use the backward Euler method for time integration with a uniform time step  $\Delta t = 0.01$ . The complete quadratic basis function is used for each element. The initial mesh is a  $16 \times 16$  uniform rectangular grid. Dynamic mesh adaptation is incorporated into the DG algorithm, and it is guided by the *a posteriori* error indicator in  $L^2(L^2)$ . A time derivative term in the interior residual is needed in the computation of the error indicator, and is approximated by a finite difference [12, 14]. The modification factor for the dynamic mesh adaptation is chosen to be  $\alpha = 0.05$ . We partition the

simulation time interval (0, 2) into 20 time slices uniformly. The iteration number is chosen to be 5 for the initial time slice and to be 2 for the remaining time slices.

Figure 6(B) shows the DG solution without mesh adaptation at  $t=1$ , whereas Figure 7 illustrates the DG solutions powered by dynamics mesh modification at various times. Due to retardation effects arising from adsorption, the contaminant transport is slower in the lower part of the domain. A continuous concentration profile is observed because of diffusion-dispersion. It should be observed that the mesh is densely refined around the moving contaminated region and at the plume front. This is driven by the physics as convection is large at high concentration area (plume center) and diffusion is significant at high concentration gradient area (plume edge). Clearly, the dynamic mesh modification guided by the  $L^2(L^2)$  error indicator sharply captures the dynamically changed local behavior of the advection-diffusion-adsorption process.

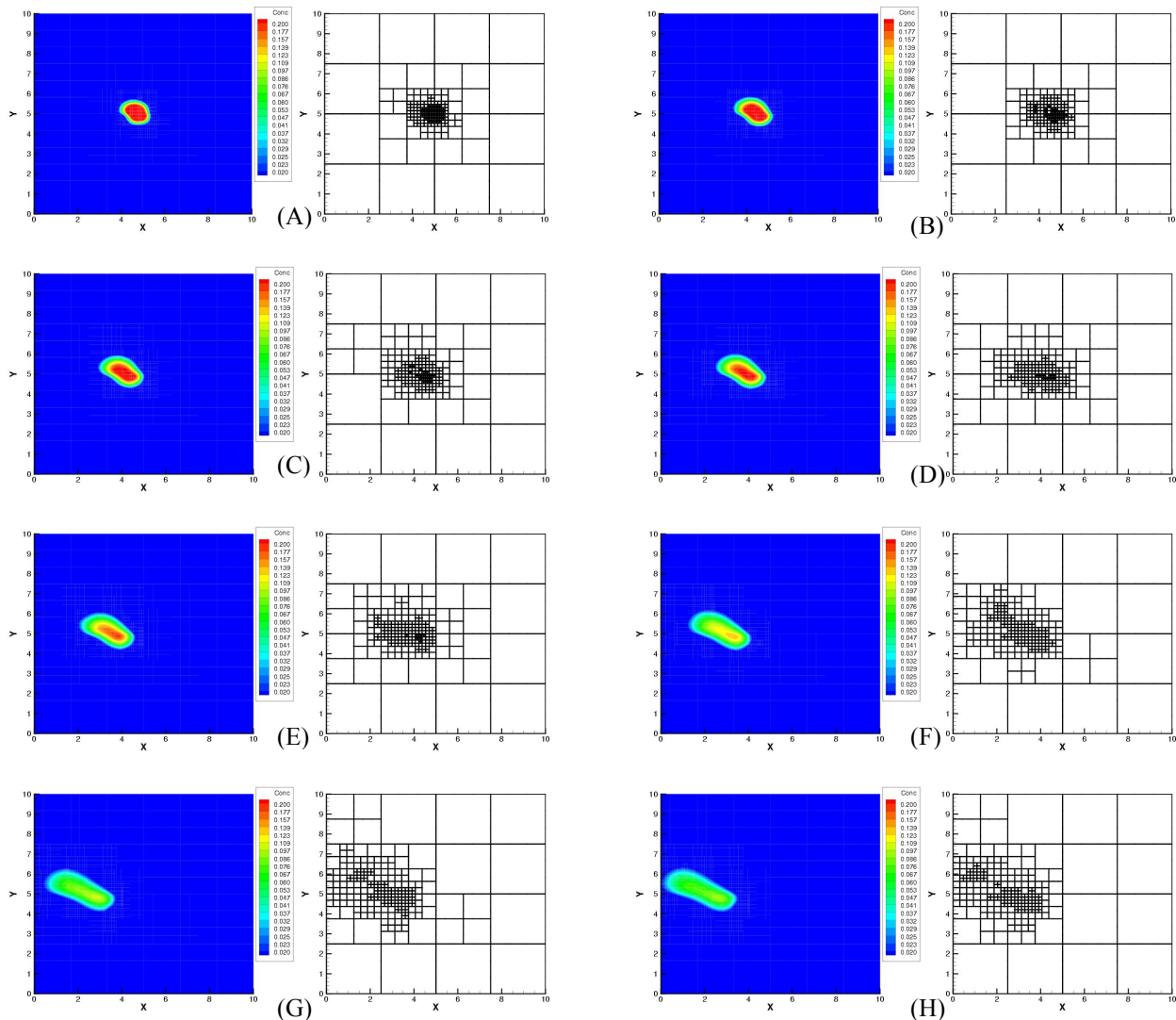


**Figure 7.** DG solutions and the mesh structures using the dynamic mesh adaptation approach at (A)  $t=0.2$ , (B)  $t=0.4$ , (C)  $t=0.6$ , (D)  $t=0.8$ , (E)  $t=1$ , (F)  $t=1.4$ , (G)  $t=1.8$ , and (H)  $t=2$ .

Due to the discontinuous space used in DG, the projections of concentration during mesh modifications involve only local computations and are locally mass conservative, which ensures both the efficiency and the accuracy of DG during dynamic mesh modifications. We emphasize that simultaneous locality of both the computation and the conservation is a unique advantage of DG, which is not satisfied by FVMs and classical FEMs. We also observe that the iteration number in each time slice can be as small as 1 or 2, which further assists the computational efficiency of DG powered by dynamic mesh adaptation.

## 6. Discussion and Conclusions

In this paper, the four primal discontinuous Galerkin methods (DG) are formulated to construct efficient solutions of parabolic type partial differential equations. Several representative example problems in chemical engineering are solved using DG. The numerical results show the capability of DG to solve a set of rather diverse time-dependent problems in chemical engineering. In addition, for mass transfer simulation, DG treats both the convection-dominated and the diffusion-dominated systems very well. For heat transfer simulation, DG is effective for both the convection-dominated and the conduction-dominated problems. DG has less numerical diffusions compared with other classic algorithms. Due to its discontinuous nature of approximation spaces, DG preserves the steep moving fronts and allows highly varied and jumped problem coefficients.

A highlight of this paper is to show that DG possesses substantial advantages on adaptive mesh modification over finite difference methods, finite volume methods and classic finite element methods. Effective adaptivity allows the attainment of accurate solutions with substantially less computational efforts. In this paper, adaptive strategies, especially the dynamic mesh modification, are formulated and studied for DG methods guided by mathematics-based and physics-driven *a posteriori* error estimators. Numerical examples demonstrate the advantage of adaptive approaches. In particular, we see that the flexibility of DG allowing non-matching meshes substantially simplifies the implementation of the mesh adaptation as the local element refinement is independent of neighborhood elements. In addition, this flexibility increases the efficiency of adaptivity because the unnecessary areas do not need to be refined just for maintaining the conformity of the mesh. Moreover, DG errors are localized; in other words, there is less pollution of errors. This leads to a more effective adaptivity for DG than for nonconforming methods. Because of this, we see that DG with adaptivity sharply captures local physical phenomena. It is also observed that the proposed dynamic strategy performs very well for transient problems with a long period of simulation time in aspects of both the accuracy and the computational cost.

## References:

- [1] M. d. C. Coimbra, C. Sereno and A. Rodrigues, "Moving finite element method: applications to science and engineering problems", *Computers and Chemical Engineering*, 28: 597-603, 2004.
- [2] C. Dawson, S. Sun and M. F. Wheeler, "Compatible algorithms for coupled flow and transport", *Comput. Methods in Appl. Mech. Engrg.*, 193: 2565-2580, 2004.

- [3] L. M. Ferreira, J. A. M. Castro and A. E. Rodrigues, "Analytical and experimental study of heat transfer in fixed bed", *International Journal of Heat and Mass Transfer*, 45(5): 937-1171, 2002.
- [4] J. T. Oden, I. Babuska, and C. E. Baumann, "A discontinuous *hp*-finite element method for diffusion problems", *J. Comput. Phys.*, 146: 491-516, 1998.
- [5] B. Riviere, M. F. Wheeler, and V. Girault, "A *priori* error estimates for finite element methods based on discontinuous approximation spaces for elliptic problems", *SIAM J. Numer. Anal.*, 39(3):902-931, 2001.
- [6] S. Sun, *Fluid mechanics behavior of liquid phase and its effects on distillation in a column containing structured packing*, Doctor of Engineering thesis, Tianjin University, 1997.
- [7] S. Sun, *Discontinuous Galerkin methods for reactive transport in porous media*, Ph.D. thesis, The University of Texas at Austin, 2003.
- [8] S. Sun, B. Riviere, and M. F. Wheeler, "A combined mixed finite element and discontinuous Galerkin method for miscible displacement problems in porous media", In: *Recent progress in computational and applied PDEs*, 321-348, July 2001.
- [9] S. Sun, S. Wang and K. T. Yu, "Effective liquid velocity in a column containing corrugated metal sheet packing", *Journal of Chemical Industry and Engineering (China: Huagong Xuebao)*, 48(6): 736-739, 1997.
- [10] S. Sun, S. Wang and K. T. Yu, "Liquid mixing behavior in a column containing structured packing", *Journal of Chemical Industry and Engineering (China: Huagong Xuebao)*, 49(1): 121-124, 1998.
- [11] S. Sun, S. Wang and K. T. Yu, "Three-dimensional simulation of distillation column containing structured packing (I) physical model and equations", *Journal of Chemical Industry and Engineering (China: Huagong Xuebao)*, Vol. 49, No. 5, pp. 549-559, 1998.
- [12] S. Sun and M. F. Wheeler, "A *posteriori* error analyses for symmetric discontinuous Galerkin approximations of reactive transport problems", *TICAM report 03-19*, Institute for Computational Engineering and Sciences, The University of Texas at Austin, Austin, Texas, 2003.
- [13] S. Sun and M. F. Wheeler, "Mesh Adaptation Strategies for Discontinuous Galerkin Methods Applied to Reactive Transport Problems", in: *Proceedings of the International Conference on Computing, Communication and Control Technologies*, H.-W. Chu, M. Savoie, and B. Sanchez, Eds., pp. 223-228, Austin, Texas, USA, August 14-17, 2004.
- [14] S. Sun and M. F. Wheeler, " $L^2(H^1)$  norm *a posteriori* error estimation for discontinuous Galerkin approximations of reactive transport problems", *Journal of Scientific Computing*, to appear.
- [15] S. Sun and M. F. Wheeler, "Discontinuous Galerkin methods for coupled flow and reactive transport problems", *Appl. Numer. Math.*, to appear.
- [16] S. Sun, A. Zeng, S. Wang and K. T. Yu, "Three-dimensional simulation of distillation column containing structured packing (II) validation of model and the effect of liquid distribution and mixing behavior on distillation", *Journal of Chemical Industry and Engineering (China: Huagong Xuebao)*, 49(5): 560-565, 1998.
- [17] M. F. Wheeler, "An elliptic collocation finite element method with interior penalties", *SIAM J. Numer. Anal.*, 15: 152-161, 1978.
- [18] M. F. Wheeler, S. Sun, O. Eslinger, and B. Riviere, "Discontinuous Galerkin method for modeling flow and reactive transport in porous media", In W. Wendland, editor, *Analysis and Simulation of Multifield Problem*, 37-58, Springer Verlag, August 2003.